Revealing the influence of additional structure on the flow field characteristics in feedwell through PIV experiments

Pengjie Wu [1,4)], Aixiang Wu [1,4*)], Zhuen Ruan [1,2,4*)], Raimund Bürger [3*)], Shaoyong Wang [1,4*)], Chong Chen[1,4)], Zhenqi Wang[1,4)]

1) Key Laboratory of the Ministry of Education of China for High-efficient Mining and Safety of Metal Mines, University of Science and Technology Beijing, Beijing 100083, China

2) Shunde Innovation School, University of Science and Technology Beijing, Foshan 528399, China

3) CI^{2}MA and Departamento de Ingeniería Matemática, Facultad de Ciencias Físicas y Matemáticas, Universidad de Concepción, Casilla 160-C, Concepción, Chile

4) School of Civil and Resource Engineering, University of Science and Technology Beijing, Beijing 100083, China

***Corresponding authors**:

Aixiang Wu, E-mail: wuaixiang@126.com;

Zhuen Ruan, E-mail: ustb_ruanzhuen@hotmail.com;

Raimund Bürger, E-mail: rburger@ing-mat.udec.cl;

Shaoyong Wang, E-mail: wangshaoyong@ustb.edu.cn.

Abstract

Cemented paste backfill (CPB) is a widely used method for resource utilization of tailings. The thickener feedwell is the key equipment for CPB in realizing solid-liquid separation. Flocculation is a significant process in treating tailings slurry thickening and dehydration. To reveal the flow field variation in the flocculation process, a range of feedwell with the additional structure were devised, containing the guide chute feedwell, the guide shelf feedwell, and the no-additional structure feedwell. To this purpose, the effects of hydrodynamics on flocculation performance in the feedwell were investigated with particle image velocimetry (PIV). The velocity and energy distribution were used to describe the variation of the flow field. The size and fractal dimension of aggregates for the flocculation reaction in the feedwell were studied. Furthermore, the turbidity was compared to evaluate the flocculation performance of these feedwells. The results of the PIV experiments indicated that the additional structure can effectively improve flocculation performance, ultimately achieving efficient solid-liquid separation efficiency. The flocculation process in the feedwell incorporates the mixing-collision section, and the settling-growth section along the flow direction, with bounding by additional structure. The ideal high-efficiency feedwell is to produce a symmetrical and uniform flow field, providing matched shear strength for the two flocculation sections. The guide shelf feedwell exhibited superior performance, resulting in

significantly larger aggregate sizes while also experiencing remarkable compactness compared to the alternative additional structure. The reason is that the tailings slurry and flocculant obtain high mixing intensity and residence time in the mixing-collision section, causing the effective collision of micro aggregates, further increasing their size and compactness in the settling-growth section. Meanwhile, the gradually decaying energy distribution avoids fragmentation of the aggregates. This work is expected to provide the theoretical basis and technical support for the design and optimization of the feedwell, finally achieving deep dewatering and reducing solid waste pollution in mines.

Keywords:

Thickener feedwell, Particle image velocimetry, Additional structure, Flow field, Flocculation performance

1. Introduction

Cemented paste backfill (CPB) is a widely used method for resource utilization of tailings[1,2]. The primary process of the CPB is to achieve the separation of tailings particles and liquid water in the slurry[3,4]. In CPB processing, the thickener is the key equipment to realizing solid-liquid separation[5-7]. By adding flocculant inner thickener feedwell, fine particles are flocculated and bridged into aggregates to accelerate sedimentation to generate clear liquid phase water (overflow) at the top of the thickener and

high concentration solid sediment (underflow) at the bottom[8-10], ultimately completing the solid-liquid separation process. In addition to tailings disposal, the solid-liquid separation with complex mechanisms exists in many industries, such as mineral processing, hydrometallurgy, oil exploitation, paper making, and wastewater treatment[5,11,12]. Although solid-liquid separation equipment in other industries has different names, such as sedimentation tank, clarifier, scrubber, etc.[13], they adopt the "particle flocculation + solid-liquid separation", which is principle similar to thickener[14].

Many scientific researchers and industry experts have reached a consensus: the feedwell is the core of the thickener[15]. The functions of feedwell mainly include: fully dissipating the initial feed kinetic energy and fully coagulating flocculant molecules and solid particles, to form large, stable, and dense aggregates[16]. The functions are achieved through its internal flow field characteristics. The flow field characteristics in the feedwell with different additional structures significantly impact the energy dissipation and particle aggregation process, thus further affecting the size and structural stability of the aggregates[17]. Therefore, it is necessary and urgent to study the flow field characteristics in the feedwell with different additional structures[6, 18].

Currently, many equipment manufacturers[19-21] and scholars have

conducted numerous researches on the flow field characteristics in the feedwell[22-24]. The flocculation behavior of the aggregates occurring in the feedwell with different process conditions and structural was investigated by small-scale physically similar models, pilot tests, and computational fluid dynamics (CFD)[25]. It was investigated that the flow field characteristics affect the flocculation efficiency in the feedwell and the operation performance of the thickener[13, 26].

In terms of the feedwell process, Ruan[27] and Wu[28] proposed a flocculation dynamics model based on the population balance by minimizing the difference between the experimental data obtained by focusing beam reflectivity measurement (FBRM) and the global optimization modeling results of aggregates. The variation of particle size distribution and underflow concentration of deep cone thickener (DCT) at different feeding speeds and solid concentrations was simulated by the model and CFD. Grabsch[16] used the same method to simulate the effects of flocculant types on the concentration of fine calcite underflow and the fractal dimension of flocs. Tanguay[29] built an open feedwell model with a shelf through CFD to simulate the effect of two flocculants on the flocculation performance in the feedwell. Wang and Cui[30-33] coupled CFD with PBM to study the impact of feed solid particle size, feed solid concentration, and feed concentration on the flocculation performance in

the thickener feedwell. Jeldres[34] obtained the structural characteristics of the aggregates and the underflow yield stress through FBRM and rheometer, respectively, to analyze the impact of the physical conditions in the feedwell (flocculant dosage and shear rate) on the underflow rheological characteristics.

In terms of feedwell structure characteristics, Owen[35] researched the influence of flocculant addition direction and speed on subsequent flocculant distribution and adsorption with CFD, thereby changing the performance of the feedwell. Based on the laser Doppler velocimetry (LDV) and tracer technology, White[36] studied the flow in the tangential feeding and the split feeding through the small-scale feedwell model, finding that the internal installation of annular plates could increase the residence time of aggregates. Mohanarangam[37] used the same experimental data to compare with the numerical prediction results and finally obtained the best turbulence model suitable for the geometry in the feedwell. Nguyen[38] designed a new feedwell model – the P266E feedwell using CFD and compared its performance with the open feedwell, the shelf feedwell, and the closed feedwell. The new feedwell can improve the stability of the flow field and underflow characteristics in the feedwell. The research on feedwell structure is mainly focused on feedwell height[39], feed pipe design[40], closed or open, etc. But to increase the residence time

of aggregates in the feedwell, industrial thickeners are often equipped with additional structures at the feedwell inlet and outlet. There is still a lack of research on the flow field characteristics and flocculation effect of additional structures.

The current research on the flow field characteristics in the thickener feedwell still mainly applies the numerical simulation[41, 42]. There is still a lack of means to obtain the flow field characteristics in the feedwell by physical experiments. The existing research mostly used LDV to measure the velocity field of small-scale physically similar models[13, 43-45]. However, LDV depends on the good tracking of tracer particles and can only obtain single-point flow field information in the feedwell. It can not represent the whole flow field information in the feedwell[46]. Particle image velocimetry (PIV) completely makes up for the limitations of single-point velocity measurement technology[47, 48]. PIV can record many velocity distribution information on spatial points in a transient state and provide a rich spatial structure of flow field and flow characteristics[48-50]. Sutalo[51] combined PIV with CFD to describe the rake's influence on the settler's fluid behavior. Alonso[52] conducted a PIV experiment and CFD on gravity settlement. The results of the PIV experiment helped improve the reliability of numerical simulation data. Currently, PIV is rarely used to study the flow field characteristics in the thickener feedwell.

To improve the internal flow field of the feedwell, investigate the effects of the additional structure on the flow field of the feedwell, and improve the flocculation efficiency, research on the influence of different additional structures in the feedwell was carried out. This study reveals the characteristics of the flow field in three different types of feedwell (guide chute feedwell (GC feedwell), guide shelf feedwell (GS feedwell), and no-additional guide structure feedwell (N feedwell)) through PIV experiments, based on the physical model of feedwell made in the laboratory. The velocity and energy distribution characteristics were used to describe the variation of the flow field. The variations in aggregate size and fractal dimension for the flocculation reaction in the feedwell were studied. Furthermore, the turbidity was compared to evaluate the flocculation performance of these feedwells.

2. Materials and methods

2.1 Experimental materials

The basic physical properties of the full tailings used in the experiment are shown in Table 1. The laser particle size analyzer was used to analyze the particle size distribution (PSD) of the tailings. The result is shown in Fig. 1. The continuous particle size (D30), median particle size(D50), and restricted particle size (D60) are 12.389 μm, 31.469 μm, and 47.835 μm, respectively. The non-uniformity coefficient and curvature

coefficient of full tailings are 17.92 and 1.20, respectively. In addition, the content of -20 μm is 39.58%, and the content of -74 μm is 69.46%. French SNF Dryfloc625V anionic polyacrylamide was selected as the flocculant in the experiment.

Table 1 Basic physical parameters of full tailings

Parameter	Density	Loose density	Dense density	Loose porosity	Dense porosity
	t/m³	t/m³	t/m³	%	%
	2.413	1.390	1.888	42.395	22.006

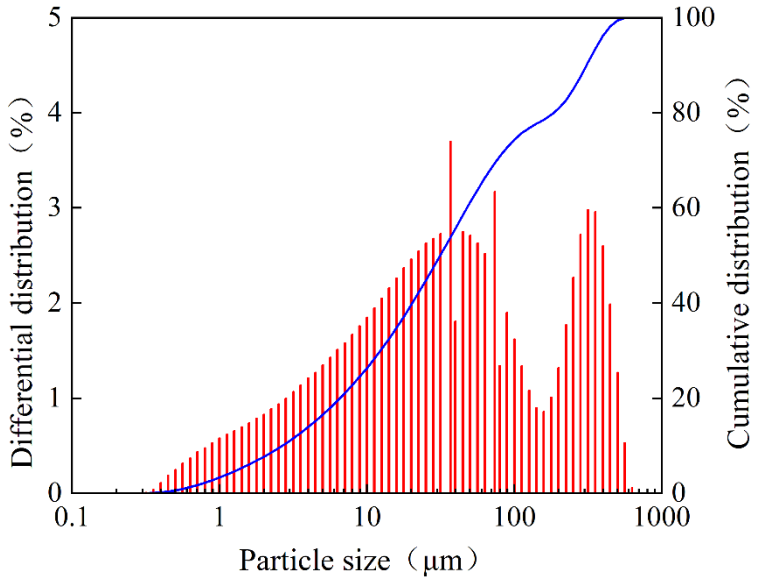

Fig. 1 The particle size distribution of full tailings

2.2 Experimental apparatus

2.2.1 Feedwell

The feedwell physical model (Feedwell system I) developed for this

study, as shown in Fig.2, is a cylindrical recipient of transparent acrylic crystal, measuring 0.2 m and 0.2 m in diameter and height, respectively. The modular design adopted by the model enables each part of the feedwell to be disassembled and assembled according to the experimental scheme. In this way, the flow field characteristics in different additional structures of feedwell can be obtained. A feed pipe was designed at a distance of 2 cm from the top, as shown in Fig. 2, measuring 6 mm and 10 mm in inner diameter and outer diameter, respectively. The feed pipe was tangent to the inner wall in the feedwell so that the tangent line of the full tailings slurry enters the feedwell.

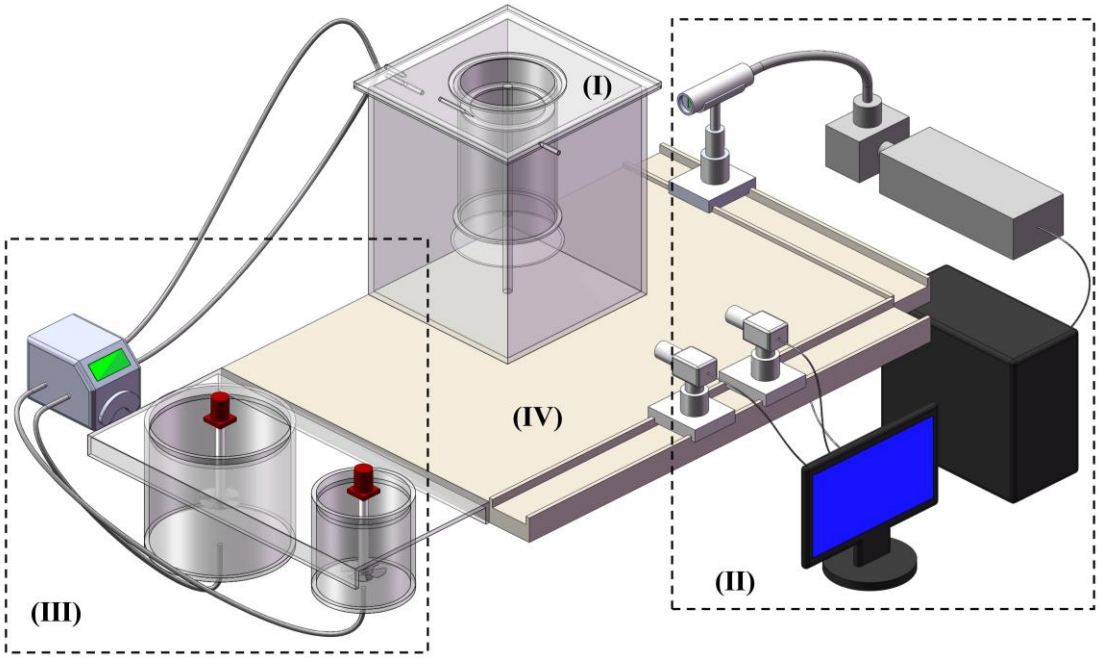

Fig. 2 Experimental apparatus: (I) feedwell system; (II) PIV system; (III) particle preparation system; (IV) experimental bench

The feedwell is usually designed as a cylinder, and the feedwell wall is a cylindrical surface[53]. Due to the scattering effect of light, curved wall will be accompanied by optical distortion when refracting laser. Optical distortions will eventually lead to out of focus of the aggregates images recorded by CCD cameras, and the effective flow field characteristics cannot be obtained[54, 55]. Therefore, to obtain clear and accurate flow field characteristics, a square sink was added outside the feedwell.

2.2.2 Additional structural module

The feedwell is the main flocculation place and core of the thickener[56]. Its different structure design will greatly affect the migration characteristics of the aggregates in the feedwell. The additional structure module contained the guide chute, guide shelf, annular shelf, and disperser.

(1) guide chute module

This module was mainly used to simulate the guide chute structure in the GC feedwell, as shown in Fig. 3 (a). The width of the bottom plate of the guide chute is 2 cm, and the helix angle is 180 °.

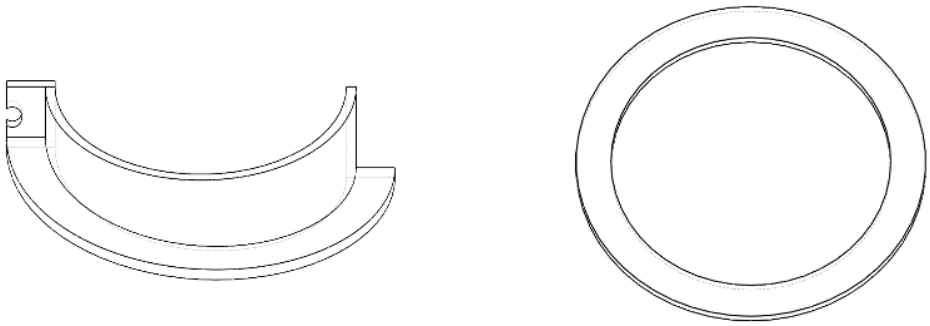

(a) (b)

Fig. 3 Additional structure module: (a)guide chute module; (b)guide/annular shelf module

(2) guide shelf/annular shelf module

In this study, the guide shelf and the annular shelf are the same components. In the GC feedwell, an annular shelf module was installed at the outlet of the feedwell to restrict the Aggregates from entering the settlement area directly from the feedwell. In the GS feedwell, a guide shelf module was installed at 1cm below the feed pipe. The full tailings slurry tangent to the feedwell can enter the lower part of the feedwell from the inner edge of the deflector only after it makes a circular movement on the guide shelf. As shown in Fig. 3 (b), the baffle is 2 cm wide and 0.5 cm thick.

(3) disperser module

The disperser module was only used in the GS feedwell. To avoid the Aggregates entering the settlement area directly from the outlet of the feedwell, a fan-shaped dispersion disk was added on the central axis. As shown in Fig. 4, the outer diameter of the bottom is 24 cm, the inner

diameter is 22.8 cm, and the angle between the bevel and the horizontal plane is 30 °.

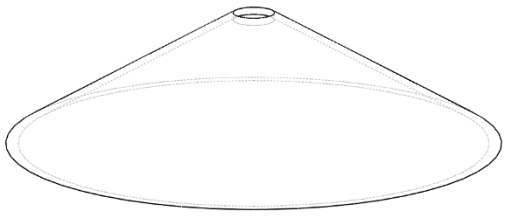

Fig. 4 Disperser module

2.2.3 PIV system

The PIV, a transient, multi-point, non-invasive hydrodynamic velocity measurement method, was developed in the late 1970s. As shown in Fig. 2, the feedwell flow field was measured by PIV (PIV system II), acquired by German LaVision Company based on a dual pulse Nd: YAG laser, laser synchronizer, Images CMOS CCD camera (2560 × 2160 pixels) and centralized control system.

2.2.4 Preparation system

Besides that, the experimental apparatus also includes a particle preparation system (III) and experimental bench (IV). The particle preparation system included a mixing tank and peristaltic pump. The particle preparation system mixed tailings and flocculant to prepare aggregates. The fluid in the feedwell was followed by aggregates that have

good fluid followability and optical properties. Besides that, the experimental apparatus also includes an experimental bench (IV). The experimental bench was used to fix the feedwell system. In addition, rails were installed on adjacent sides of the experimental bench to install laser and CCD cameras respectively. That could ensure that the laser light source and CCD camera are vertical to obtain clear flow field images.

2.3 Experimental procedure

Table 1

Experimental conditions and parameters

Feedwell type	Additional structure		Feed flow	Slurry concentration	Flocculant unit consumption
	feed pipe	outlet			
GC feedwell	guide chute	annular shelf	2700mL/min	10 %	40 g/t
GS feedwell	guide shelf	disperser			
N feedwell	no structure	no structure			

The feedwell of different additional structures can be formed by matching different modules. According to the existence and types of additional structures, the flow field characteristics in three types of feedwell were studied in this paper. As shown in Fig. 5: In the GC feedwell, a guide chute was installed at the tangent feed pipe, and an annular shelf was installed at the outlet of the feedwell module. The GS feedwell was equipped with a guide shelf at the tangent feed pipe and a fan-shaped disperser at the outlet of the feedwell module. In contrast, the N feedwell did not equip any additional structure. The experimental parameters are

presented in Table 1, and remained consistent during the experiment.

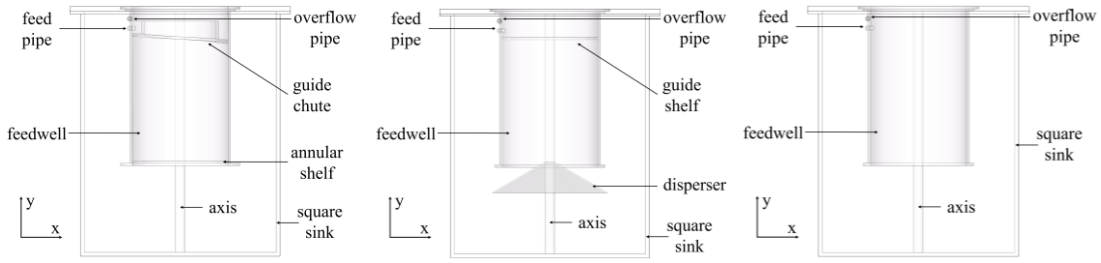

(a) (b) (c)

Fig. 5 Different additional structure types of feedwell models(CCD camera view: meridional plane): (a) GC feedwell; (b) GS feedwell; (c) N feedwell

2.4 Evaluation index

The image pairs obtained from the PIV experiments were organized and velocity fields were calculated with an embedded toolbox-Davis. A cross-correlation algorithm was used with an interrogation window size of 32 × 32 pixels, with an overlap of 50%. The performance of Aggregates was performed using ImageJ and Origin.

(1) Velocity field distribution

In this paper, the time-averaged velocity field was used to characterize the velocity distribution of different types of feedwell. The velocity field obtained by the cross-correlation algorithm can be expressed by combined velocity (V), axial velocity (v), and radial velocity (u) respectively. As shown in Fig. 5, the axial velocity v is the component velocity in the central axis direction Y, and the radial velocity u is the velocity component in the

feedwell diameter direction X.

(2) Turbulent kinetic energy distribution

From the time series of u and v fields, the turbulence kinetic energy(k) was calculated as:

$$k=\frac{1}{2}(2u^2+v^2) \tag{1}$$

This paper focused on the distribution of turbulent kinetic energy(k) in the tangent feeding section and at the outlet of the feedwell. To characterize the TKE dissipation capacity in the feedwell, the attenuation rate of $k(\varepsilon)$ was defined[46]. The formula is as follows.

$$\varepsilon=\frac{k_0-k_1}{k_0} \tag{2}$$

Where ε represents the attenuation rate of k, and k_0 represents the k in the feeding section of the feedwell，k_1 represents the k at the feedwell outlet.

(3) Characterization of flocculated aggregates

The projected area A and perimeter P of aggregates were obtained by using ImageJ to segment the image threshold. The equivalent particle size d of the aggregates was calculated as

$$d=(\frac{4A}{\pi})^{0.5} \tag{3}$$

To avoid the statistical error caused by uneven particle distribution, the particle size of aggregates under the same test condition was collected and the mean particle size D was calculated as the evaluation index.

The fractal dimension D_F of aggregates is related to the projected area and perimeter. D_F can be calculated as follows

$$A=\alpha P^{D_F} \tag{4}$$

$$\ln A = D_F \ln P + \ln \alpha \tag{5}$$

3. Results and discussion

3.1 Effect of additional structure on the velocity field

3.1.1 Effect of additional structure on the vector velocity

The structure of the feedwell affects the velocity field, which further influences the uniform mixing and effective collision of tailings particles. The meridian plane of the feedwell is displayed in Fig. 5, which is perpendicular to the tangent feed pipe and passes through the central axis of the feedwell. The tailings slurry and flocculant solution entered the feedwell tangentially from the feed pipe with the largest initial kinetic energy, so the distribution of the large velocity has been observed in the upper left of the measured area on the meridian plane, as is shown in Fig. 6.

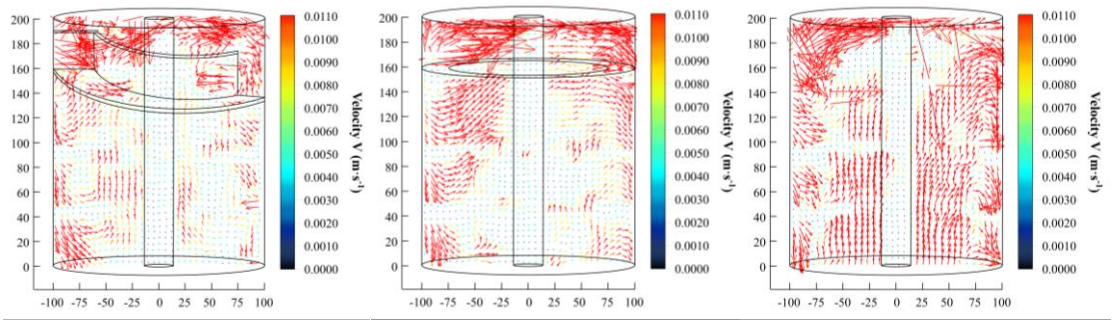

(a) (b) (c)

Fig.6 Vector velocity distribution in feedwell with different additional structures: (a)GC feedwell；(b)GS feedwell；(c)N feedwell

The distribution of the vector velocity in the feedwell with different additional structures is shown in Fig. 6. When the feedwell has an additional structure, the fluid exhibits the all-field distribution of the high vector velocity above the additional structure of the feedwell, with insignificant radial attenuation. The larger the vector velocity inner the additional structure, the greater the mixing intensity generated in the fluid, which is beneficial for the dispersion of flocculant in the slurry, and will also enhances the collision between particles. Therefore, the additional structure is the core place where the flocculation process occurs in the feedwell, and the large vector velocity distribution appearing in the additional structure is conducive to improving particles collision and bridging flocculation. As the fluid flows out of the additional structure, the GC feedwell and the GS feedwell exhibit different local distribution. There is no large velocity distribution near the guide chute of the GC feedwell, whereas large velocity distribution is still observed at the inner edge and the bottom plate of the guide shelf in the GS feedwell. The appearance of large upward velocity indicates a significant velocity gradient at the inner edge of the guide shelf, which causes a backflow phenomenon. The backflow phenomenon in the guide shelf is a double-edged sword for the

flocculation process, which may be beneficial to increase the effective collision of tailings particles, thereby improving the flocculation efficiency of the feedwell. On the contrary, the excessive mixing intensity appearing at the outlet of the additional structure may also potentially lead to the fragmentation of already formed aggregates.

Upon entering the lower part of the additional structure in the feed well, the structure and direction of the flow field in the GC feedwell and GS feedwell were observed to be similar, with the highest velocity near the sidewall, gradually decreasing along the radius direction toward the center axis. Compared with the upper part of the feedwell additional structure, the spatial extent of the fluid motion significantly decreases, the vector velocity shows high values near the wall and low values around the center axis. The fluid performs swirling motion on the wall, with the vector velocity is obviously smaller than that in the additional structure. The distribution characteristics indicates that the mixing intensity in feedwell is significantly reduced, which is conducive to the gradual growth of aggregates and prevents the breakage of the formed aggregates.

Contrastingly, the vector velocity of the N feedwell was larger at the left wall of the upper feed section, which is the tangential feed pipe, while the vector velocity gradually decreased along the radius direction toward the right wall. After the slurry entered the feedwell tangentially from the

feed pipe, it did not stay too much at the upper feed section, and it dropped rapidly along the feedwell wall. There was not a wide range of fluid near the central axis of the N feedwell. Compared with other feedwell, the dead water zone in the upper feed section of the N feedwell was larger. The velocity near the central axis was found to be larger in the N feedwell, with a wider distribution, while the velocity distribution range at the feedwell wall was narrow. This was prone to short-circuit backflow areas at the exit of the feedwell.

According to the distribution features of the velocity field, the feedwell is divided into a mixing-collision section and a settling-growth section by taking the installation position of the additional structure as the feature boundary line. To examine the impact of the additional structure on the vector velocity distribution, the vector velocity distribution near the boundary line is selected for analysis. As illustrated in Fig. 7, the guide chute enhances the uniform distribution and symmetry of the flow field. Poor flow field symmetry can result in uneven mixing effects, leading to non-uniform distribution of flocculants and tailings particles, thus reducing flocculation efficiency.

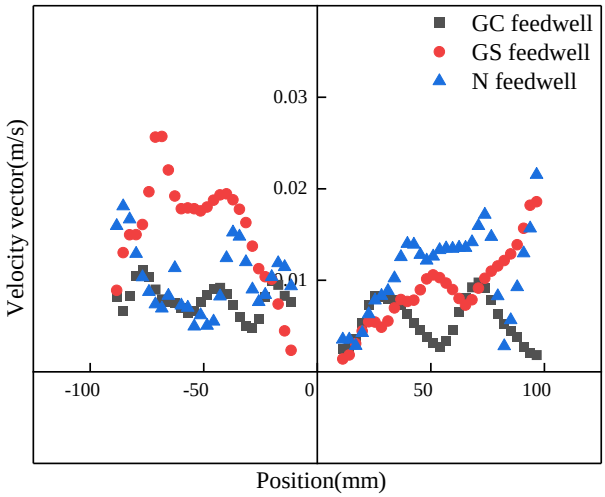

Fig. 7 Vector velocity distribution of feature boundary line in feedwell

3.1.2 Effect of additional structure on the radial velocity

The cloud chart of the radial velocity distribution is presented in Fig. 8. The radial velocity represents the rotational intensity of the fluid, a high radial velocity indicates a high mixing intensity, which is favorable for particle collision. As illustrated in Fig. 8, a whole-field distribution of large radial velocity is observed in the mixing-collision section of the GC feedwell and GS feedwell, indicating a counterclockwise rotational motion of the fluid in the additional structure, which is beneficial to provide high mixing strength for particle collision and flocculant dispersion. Upon the fluid enters the feedwell tangentially, it makes a spiral motion under the guidance of the guide chute, and makes a circular motion under the flow limiting effect of the guide shelf, respectively in the GC feedwell and GS feedwell. As the fluid moves downward into the settling-growth section,

the radial velocity significantly decreases in the GC feedwell, leading to a reduction in rotational intensity. The reduction in rotational intensity in the tangential direction promotes the growth of existing micro aggregates and prevents the breakage of newly formed micro aggregates. But in the GS feedwell, the high radial velocity is still observed near the bottom plate of the guide shelf, with the large fluid movement range in the settling-growth section, insignificantly decreasing along the flow direction towards the outlet. The high radial velocity appearing in the settling-growth section may potentially lead to the fragmentation of already aggregates. Compared with the additional structure feedwell, the N feedwell had no additional feed structure that limits the radial movement of the slurry in the mixing-collision section. Therefore, the radial velocity of the N feedwell is only distributed on the feedwell wall with the small spatial extent of the fluid motion. Especially in the mixing-collision section, the dead zones with zero radial velocity appear near the center axis, disrupting the overall symmetry and uniformity. This is not conducive to the uniform dispersion of the flocculants and the collision-attachment of particles, resulting in many fine tailings not effectively flocculating.

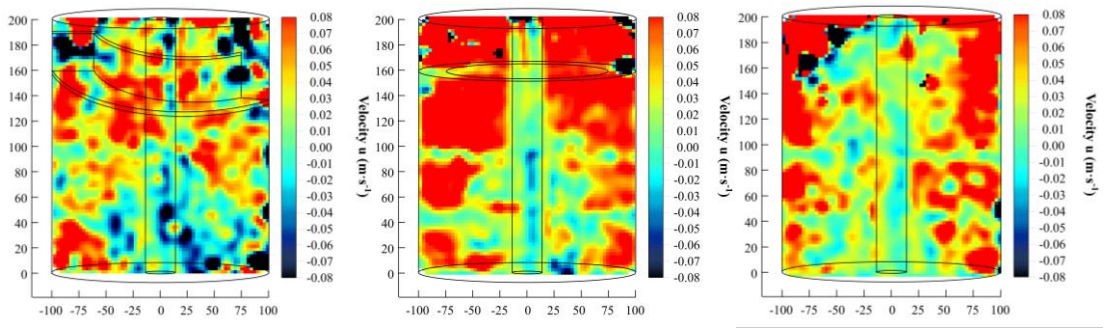

(a) (b) (c)

Fig. 8 Radial velocity distribution in feedwell with different additional structure: (a)GC feedwell；(b)GS feedwell；(c)N feedwell

To examine the impact of the additional structure on the radial velocity distribution, the radial velocity distribution near the feature boundary line is selected for analysis. From Fig. 9, it can be observed that additional structure has maximum impact on the radial velocity distribution. The addition in structure significantly increases the fluid's radial velocity after entering the reactor. Indeed, the reason for this is that it affects the duration of swirling motion of the fluid in the mixing-collision section. Compared with the GC feedwell, the GS feedwell has a more obvious impact on the radial velocity value, but the guide shelf destroys the symmetry of the radial velocity in the mixing-collision section. Poor flow field symmetry can result in uneven mixing effects, leading to non-uniform distribution of flocculants and particles, thus reducing flocculation. The GC feedwell exhibits excellent uniformity and symmetry in the radial velocity. It provides high mixing strength in the guide chute and prolongs

the residence time of the fluid in the mixing-collision section. These advantages promote the formation of small aggregates. The distribution pattern in the N feedwell shows a more pronounced trend of rapidly decreasing radial velocity along the feature boundary line, which meant that upon the fluid enters the feedwell, it quickly enters the settling-growth section and does not stay in the mixing-collision section. This can result in disrupting the fluid symmetry and uniformity, ultimately influencing the efficiency of flocculation.

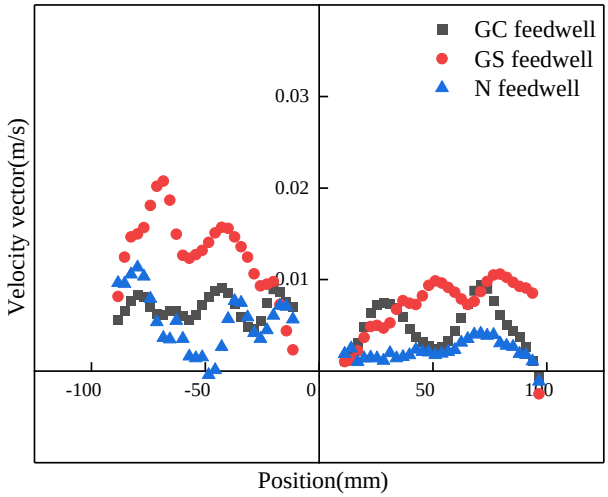

Fig. 9 Radial velocity distribution of feature boundary line in feedwell

3.1.3 Effect of additional structure on the axial velocity

Fig.10 exhibit the axial velocity distribution of the feedwell with the different additional structures. The structure and direction of the axial velocity fields in feedwell with different additional structure were observed

to be similar, with the polarized and symmetric distribution, showing the upward axial velocity distribution adjacent to the center axis, and the downward axial velocity distribution in proximity to wall. Compared with additional structure feedwell, the axial upward velocity value near the central axis of the N feedwell is the largest, with the widest distribution range. This demonstrates the formation of backflow in the center of the N feedwell, which increases the mixing intensity of the settling-growth section in the N feedwell, and the aggregates formed in the mixing-collision section become loose and prone to fragmentation, resulting in small aggregates.

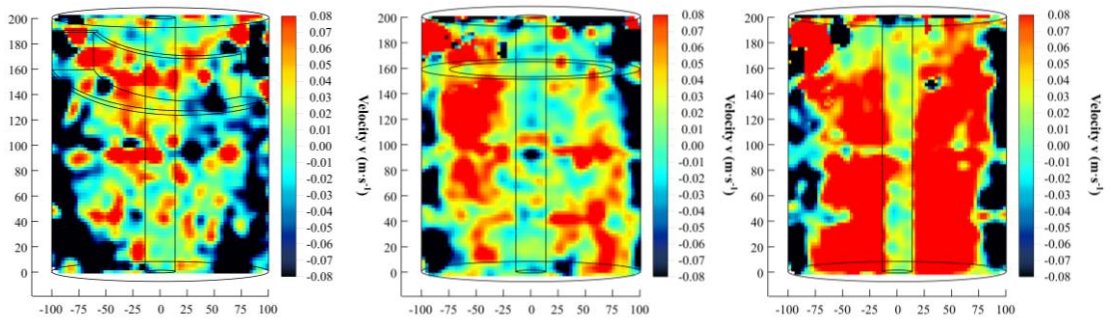

(a) (b) (c)

Fig. 10 Axial velocity distribution in feedwell with different additional structure: (a)GC feedwell；(b)GS feedwell；(c)N feedwell

As shown in Fig. 11, the additional structure has a significantly effect on the axial velocity distribution in feature boundary line. The guide chute significantly decreases the axial velocity in the GC feedwell, resulting in an increased residence time of the fluid in the mixing-collision section, and

a reduction of short circuit reflow phenomena. When the additional structure is the guide chute, the axial velocity becomes uniform and symmetrical, and an obvious decrease in axial velocity along the flow direction is observed. This results in a uniform flow of slurry and flocculant in the axial direction, which will facilitate their sufficient mixing and avoiding breakage of aggregates. When the additional structure is guide shelf, the high value of the axial upward velocity has been observed in the second quadrant, which illustrates that the fluid flows back into the mixing-collision section. Indeed, due to the limited flow restriction effect of the guide shelf and the large initial kinetic energy, part of the fluid enters the guide shelf tangentially and directly enters the settling-growth section from the mixing-collision section, with a large velocity gradient at the feature boundary line. The obvious short-circuit backflow phenomenon destroys the symmetry and uniform distribution of the flow field in the GS feedwell. Compared with the GC feedwell, the axial velocity of the wall in the GS feedwell and N feedwell increases significantly. The increase in axial velocity reduces the residence time of the fluid in this area, leading to insufficient mixing between the slurry and the flocculant, and the flocs become loose and prone to fragmentation, resulting in small aggregates.

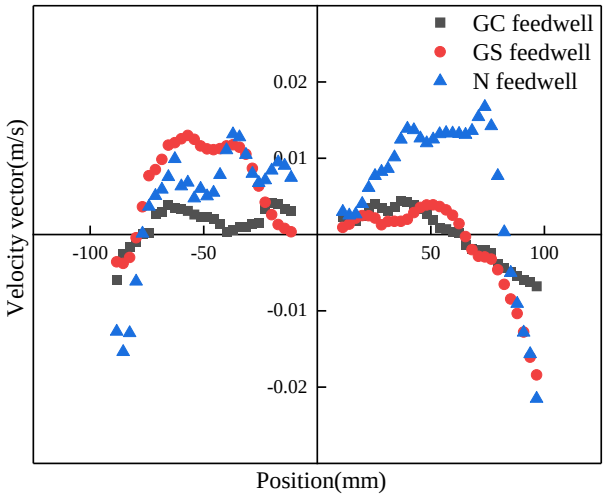

Fig. 11 Axial velocity distribution of feature boundary line in feedwell

3.2 Effect of additional structure on the energy distribution

3.2.1 Effect of additional structure on the turbulent kinetic energy

The *k* distribution of fluid field in the feedwell with different additional structure is shown in Fig.12. The structure and strength of the *k* in the feedwell reflect the distribution of the shear intensity of the flow field from the perspective of kinetic energy, with high values indicating a high degree of fluid mixing[57,58].

In the GC feedwell, a significant distribution characterized by high *k* value materialized in the mixing-collision section, and a lower k distribution in the settling-growth section, with the *k* value gradually decreasing along the flow direction of the fluid. This results in a more

symmetrical and uniform distribution within the feedwell, aligning with the energy requirements at different stages of aggregates growth during the flocculation process. On the one hand, the tailings and flocculant are fully diffused and effectively collided upon the high k value in the mixing-collision section, with better flocculation efficiency. The k value decays rapidly in the guide chute, which illustrated that the main place where flocculation behavior occurred in the GC feedwell is the guide chute. On the other hand, the aggregates that have been flocculated are not destroyed by excessive shear upon the lower k value in the settling-growth section, resulting in the micro aggregates form the densely structured aggregates.

In the GS feedwell, there is negligible change for the k distribution in the mixing-collision section, with comparing with the GC feedwell, but a chaotic distribution is illustrated in the settling-growth section. The high k value is not only observed in the mixing-collision section, but there is also concentrated at the bottom plate of the guide shelf in the settling-growth section. The upper and lower areas of the guide shelf are the core areas where flocculation behavior occurred in the GS feedwell. This can result in a short circuit phenomenon near the inner edge of the guide shelf, and the micro aggregates that have been formed return the mixing-collision section with the reflux fluid. As mentioned earlier, this distribution pattern results in excessive shearing that may causes the decomposition of the

aggregates.

The high *k* value of the N feedwell is distributed on the wall of the feedwell, which is shown in Fig.12(c). In the N feedwell, dead zones with low turbulence intensity appear nearby the center axis in the mixing-collision section. This is not conducive to the uniform dispersion of the flocculants and the collision attachment of tailings, resulting in many particles not effectively flocculating. After the slurry enters the feedwell tangentially, it spirally moves along the feedwell wall and leaves the mixing-collision section. However, the high *k* value is still observed in the settling-growth section, disrupting the overall symmetry and uniformity. This leads to ineffective collisions of the micro aggregates generated in the mixing-collision section when they enter the settling-growth section, which is unfavorable for floc growth.

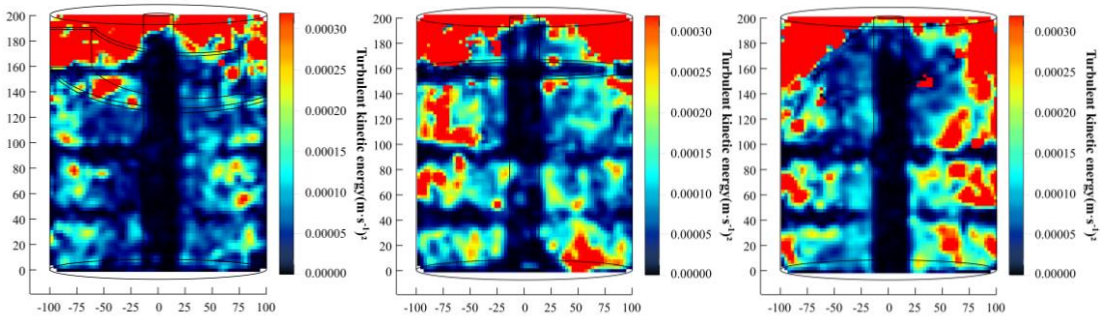

(a) (b) (c)

Fig. 12 Turbulent kinetic energy distribution in feedwell with different additional structure: (a)GC feedwell；(b)GS feedwell；(c)N feedwell

3.2.2 Effect of additional structure on the turbulent attenuation

The slurry enters the feedwell tangentially with a large flow rate, forming a high-strength shear zone in the mixing-collision section. The definition of an efficient feedwell is to utilize the mixing strengthen to promote the diffusion of tailings particles and flocculant, with capturing the fine tailings for flocculation, finally producing a warm and uniform fluid at the outlet of the feedwell. If the aggregates enter the thickener sedimentation area at a high velocity, short circuit backflow and mudding may be observed in the thickener, ultimately affecting the solid-liquid separation efficiency.

Fig.13 exhibits the *k* distribution at the outlet of three additional structures of the feedwell, which intuitively reflects the turbulent kinetic energy dissipation of the feedwell[59,60]. The high *k* value is still observed on the surface of the disperser disk in the GS feedwell. The aggregates discharged from the feedwell collides and slides on the surface of the dispersion module, temporarily generating relatively large *k*. There is still a high *k* distribution at the outlet of the N feedwell. The aggregates spirals down so rapidly along the feedwell wall that the turbulent is not fully dissipated. Furthermore, the high *k* distribution at the outlet of the feedwell indicates that aggregates leave the feedwell with a faster velocity and enter the thickener settlement area, with impacting the stable mud layer formed

at the bottom of the thickener, eventually leading to turbidity. Contrastingly, in the GC feedwell, the aggregates move spirally downward along the feedwell wall under the guidance of the guide chute, with gradually dissipating turbulent, resulting in no high k value at the outlet of the feedwell.

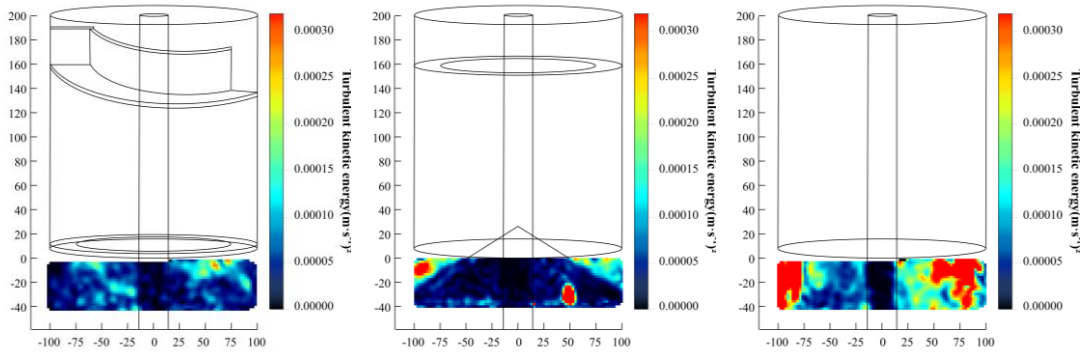

(a) (b) (c)

Fig. 13 Turbulent kinetic energy distribution at the outlet in feedwell: (a)GC feedwell；(b)GS feedwell；(c)N feedwell

The key function of the feedwell is to dissipate the initial kinetic energy of the feed. The turbulence attenuation reflects the efficiency of converting turbulence energy into the energy required for particle collision and mixing in the flocculation process. The ε calculated by the formula (2) in the GC feedwell, GS feedwell, and N feedwell are 97.38%, 95.36%, and 85.64% respectively. For the same initial feed kinetic energy, the ε of the N feedwell is the lowest, while the ε of the GC feedwell and the GS feedwell are relatively optimal. The GC feedwell has an increase of 11.74%

compared to the N type feed well, and the GS feedwell has an increase of 9.72%. For identical flocculation conditions, adding additional structures downstream of the feed pipe and at the outlet of the feed well, will effectively improve the ability to dissipate turbulent. The favorable attenuation capabilities help allows the flocculant to be more evenly dispersed in the slurry, providing suitable energy input for different stages of aggregates growth, ultimately achieving high flocculation efficiency.

3.3 Effect of additional structure on the flocculation performance

D_{50} and D_F are served as a quantitative measure of aggregates size and compactness respectively, with turbidity indicating fine particle adsorption capacity, ultimately reflect the flocculation performance[61,62]. The D_{50} are 348.85, 332.79, and 280.24 μm corresponding to GC, GS, and N feedwell, respectively, with the D_F are 1.58, 1.50, and 1.52. Turbidity is 23.6ppm, 55.2ppm, 126.8ppm, respectively.

As shown is Fig. 14, the D_F in the GC feedwell is the largest, with the most stable structure, highest fine particle removal efficiency. In summary, the tailings reacted fully in the guide chute of the GC feedwell and were not excessively sheared in the settling section. The aggregates formed in the GC feedwell had the largest particle size with the most stable structure. The GC feedwell exhibits a dense aggregates structure with a larger final aggregates size compared to other feedwell. The reason is that the tailings

slurry and flocculant obtain high mixing intensity and residence time in the mixing-collision section, causing the effective collision of micro aggregates. These micro aggregates undergo effective collision further increase their size and compactness in the settling-growth section. Meanwhile, the gradually decaying energy distribution avoids fragmentation of the aggregates.

As shown in Fig. 14, the aggregates are large but loose in the GS feedwell. The D_{50} and the D_F are 332.79 μm and 1.50, respectively. The turbidity is 55.2 ppm. The results indicate that the size of the aggregates formed by the GS feedwell is larger, but the structure of the aggregates was unstable. This performance may be attributed to the poor symmetry velocity distribution and the high energy distribution in the settling-growth section. Although the tailings particles and flocculants can undergo effective mixing and collision in the guide shelf, the formed micro aggregates cannot further growth when the aggregates enter the settling-growth section and aggregates are susceptible to fragmentation in the settling-growth section, resulting in the loose aggregate.

In the N feedwell, D_{50} and the D_F are 280.24 μm and 1.52, respectively, and the turbidity increases to 126.8. These are due to the reducing residence time for the fluid in the mixing-collision part, which results in inadequate mixing of tailings and flocculants, ultimately

producing micro and loose aggregates.

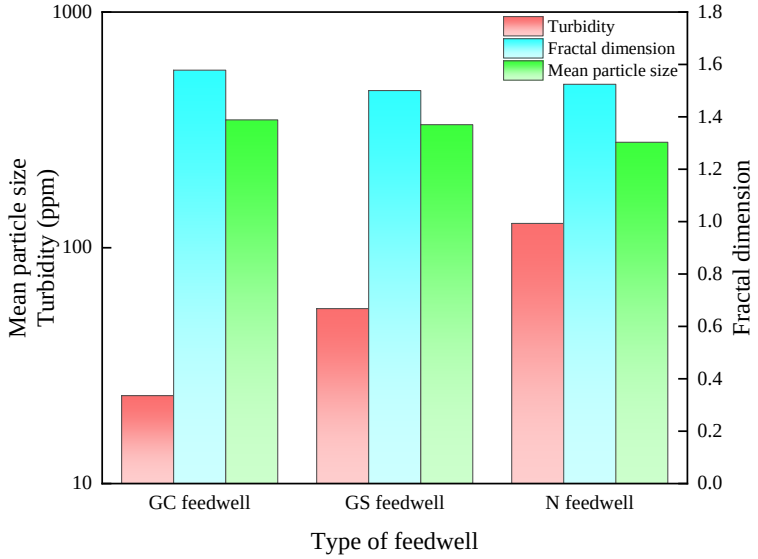

Fig. 14 Flocculation performance of the feedwell with different additional structure

3.4 Flocculation mechanisms comparison

Fig. 15 illustrates the streamline distribution of the fluid and flocculation mechanism in the feedwell with different additional structures. The additional structure is essential to ensure optimal conditions for flow field shear and energy transfer in the feedwell, ultimately beneficial to the growth of tailings particles.

The tailings slurry and flocculant enter the upper mixing-collision section of the GC feedwell through the tangential feed pipe, with carrying a large initial kinetic energy. The aggregates do not leave the mixing-collision section directly upon the aggregates enters the GC feedwell, but mixed and collided in the guide chute to fully dissipate the turbulent kinetic energy, as shown in Fig. 15(a). Then, the aggregates make a spiral motion

along the wall under the diversion effect of the guide chute, finally leaving the feedwell at a gentle speed and entering the thickener settlement area. The velocity and turbulent kinetic energy distribution inner the guide chute of the GC feedwell were the largest, which illustrated that the main place for the Aggregates flocculation and bridging process is the guide chute, which has the highest shear strength. The GC feedwell exhibits excellent uniformity and symmetry in the flow field. It provides high mixing strength in the mixing-collision section and prolongs the residence time of the particles and flocculant in this region. These advantages enhance the bridge of flocculants with particles and the collision of micro aggregates, thereby promoting the formation of micro and loose aggregates. Moreover, the velocity and energy distribution in the settling-growth are minimal, thereby preventing the breakage of already formed aggregates and facilitating the capture of fine particles by existing aggregates, causing the development of large and dense flocs. Therefore, the GC feedwell facilitates particles collision and aggregates growth, resulting in large aggregates sizes with high compactness, thereby achieving a high flocculation efficiency

When the tailings slurry and flocculant enter the upper mixing-collision section of the GS feedwell, the streamline of fluid is similar to that of the GC feedwell. The guide shelf is the core region where flocculation occurs in the GS feedwell. The aggregates make a circular

motion in the mixing-collision section under the flow restriction of the guide shelf, as shown in Fig.15(b). Subsequently, the aggregates leave the mixing-collision from the inner edge of the guide shelf and move spirally downward along the wall. Due to the restriction of the guide shelf, part of the fluid randomly leaves the mixing-collision section from the inner edge of the shelf, and multiple streams of fluid make spiral motion in the lower part. Due to the restriction effect of the guide shelf is limited, part of the fluid randomly leaves the mixing-collision section from the inner edge of the guide shelf, and the initial fluid is divided into multiple streams of fluid and performs spiral motion on the wall. The micro and loose aggregates enter the settling-growth section from the inner edge of the guide shelf at a higher speed, with generating a velocity gradient on the inner edge of the guide shelf, causing the liquid water to backflow. Part of the micro and loose aggregates enter the mixing-collision section again with the backflow water, indicating that there is a short-circuit near the guide shelf of the GS feedwell. This distribution pattern destroys the overall symmetry and uniformity of the flow field, with providing too high mixing intensity in the mixing-collision, eventually leading to excessive shearing of aggregates. and the aggregates become loose and easily broken, eventually producing large and loose aggregates. The aggregates produced in the mixing-collision section become loose and prone to fragmentation,

resulting in large but loose aggregates.

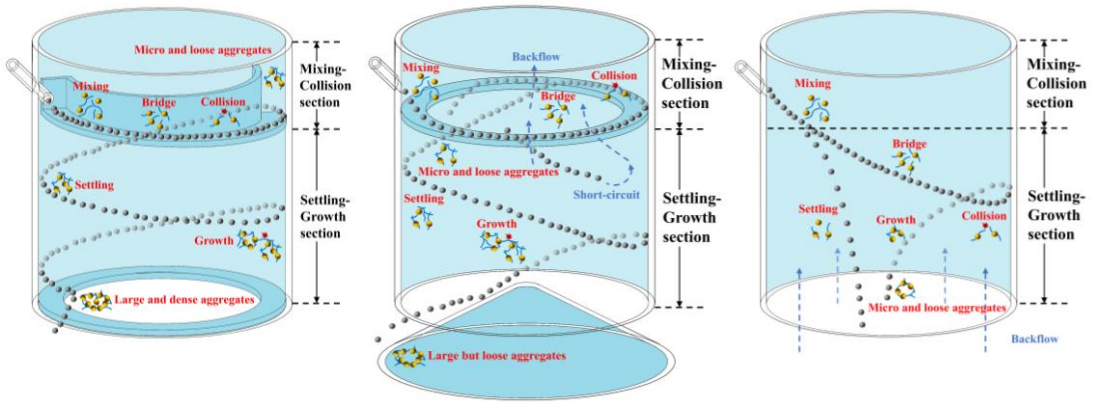

(a) (b) (c)

Fig. 15 The streamline of fluid and flocculation mechanism in the feedwell with different additional structures: (a)GC feedwell; (b)GS feedwell; (c)N feedwell

Fig.15(c) shows the streamline and flocculation mechanism in the N feedwell. Due to without any structures to restrict the slurry, slurry does not stay in the mixing-collision section but spirals rapidly down along the wall of the feedwell under the action of initial kinetic energy. The dead zones with low velocity and turbulence intensity appear in the mixing-collision section, disrupting the overall symmetry and uniformity. This is not conducive to the uniform dispersion of the flocculants and the collision attachment of tailings particles, resulting in many fine particles not effectively flocculating. What's more, the aggregates leave the feedwell along the wall with greater kinetic energy, and there is a pressure difference at the outlet of the feedwell. A large amount of liquid water carrying fine particles back flow into the feedwell. There are some issues still existing

in the N feedwell, including poor symmetry of the flow field distribution, weak mixing intensity, and the presence of dead zones, ultimately producing micro and loose aggregates.

In general, the feedwell incorporates mixing-collision section, and settling-growth sections along the central axis direction, with bounding by additional structure. The feedwell with superior performance generates a symmetrical and progressively decreasing flow field distribution along the flow direction, supplying the matching shear intensity for two flocculation stages. Based on the above experimental results and discussions, the GC feedwell with the additional structure of the guide chute exhibited superior performance, with resulting in significantly larger aggregates sizes, while also experiencing remarkable compactness compared to alternative additional structure. The GC feedwell showed remarkable flocculation performance with high turbidity. It needs to be emphasized is that inference has certain limitations, with inferring through the existing flocculation conditions and structural parameters. To ensure the consistency of experimental conditions, parameters were kept consistent during the flocculation process. However, the chosen parameters may not be optimal for the feedwell with the additional structure. Optimizing the structural parameters and flocculation conditions of the feedwell is the next research work, ultimately developing an ideal feedwell that can provide efficient

and sustainable treatment for industry-wide of solid-liquid separation process.

4. Conclusions

This study explored the impacts of the additional structures in the feedwell on the characteristics of the flow field and flocculated particle aggregates.

(1) The additional structure can enhance symmetry and uniform distribution of flow fields, effectively improving flocculation performance, ultimately achieving efficient solid-liquid separation efficiency.

(2) The flocculation process in the feedwell incorporates the mixing-collision section, and the settling-growth section along the flow direction, with bounding by additional structure. The ideal high-efficiency feedwell is to produce a symmetrical and uniform flow field, providing matched shear strength for the two flocculation sections.

(3) The GC feedwell exhibited superior performance, resulting in significantly larger aggregate sizes while also experiencing remarkable compactness compared to the alternative additional structure. The reason is that the tailings slurry and flocculant obtain high mixing intensity and residence time in the mixing-collision section, causing the effective collision of micro aggregates, further increasing their size and compactness in the settling-growth section. Meanwhile, the gradually decaying energy

distribution avoids fragmentation of the aggregates, ultimately achieving solid-liquid separation.

(4) The results obtained herein extend the existing knowledge of the thickener solid-liquid separation process from a hydrodynamic point of view and provide a basis for the further development of additional structures for the feedwell.

Acknowledgment

This research was funded by the National Natural Science Foundation of China (no.52130404), Guangdong Basic and Applied Basic Research Foundation (no. 2021A1515110161), the Fundamental Research Funds for the Central Universities (no.FRF-TP-22-112A1), ANID (Chile) through Fondecyt project 1210610, Centro de Modelamiento Matemático (BASAL funds for Centers of Excellence FB210005), CRHIAM project ANID/FONDAP/15130015, and Anillo project ANID/ACT210030.

References

[1] Wu A, Ruan Z, Wang J. Rheological behavior of paste in metal mines[J]. International Journal of Minerals, Metallurgy and Materials, 2022, 29(4): 717-726.

[2] Jiao H, Yang W, Ruan Z, et al. Microscale mechanism of tailing thickening in metal mines[J]. International Journal of Minerals, Metallurgy and Materials, 2023, 30(8): 1538-1547.

[3] Chen G, Li C, Ruan Z, et al. Research on floc structure and physical properties based on pipeline flocculation[J]. Journal of Water Process Engineering, 2023, 53: 103627.

[4] Jiao H, Chen W, Wu A, et al. Flocculated unclassified tailings settling efficiency improvement by particle collision optimization in the feedwell[J]. International Journal of Minerals, Metallurgy and Materials, 2022, 29(12): 2126-2135.

[5] Qi C, Fourie A. Cemented paste backfill for mineral tailings management: Review and future perspectives[J]. Minerals Engineering, 2019, 144: 106025.

[6] Cheng H, Liu J, Wu S, et al. Fluidization Analysis of Thickening in the Deep Cone for Cemented Paste Backfill[J]. Advances in Materials Science and Engineering, 2020, 2020.

[7] Jiao H, Wu Y, Wang H, et al. Micro-scale mechanism of sealed water seepage and thickening from tailings bed in rake shearing thickener[J]. Minerals Engineering, 2021, 173: 107043.

[8] Wang S, Song X, Wang X, et al. Influence of coarse tailings on flocculation settlement[J]. International Journal of Minerals, Metallurgy and Materials, 2020, 27: 1065-1074. [9] Usher S P, Scales P J. Steady state thickener modelling from the compressive yield stress and hindered settling function[J]. Chemical Engineering Journal, 2005, 111(2-3): 253-261.

[10] Das S, Bai H, Wu C, et al. Improving the performance of industrial clarifiers using three-dimensional computational fluid dynamics[J]. Engineering Applications of Computational Fluid Mechanics, 2016, 10(1): 130-144.

[11] Wu A, Ruan Z, Wang J. Rheological behavior of paste in metal

mines[J]. International Journal of Minerals, Metallurgy and Materials, 2022, 29(4): 717-726.
[12] Chen Q, Tao Y, Zhang Q, et al. The rheological, mechanical and heavy metal leaching properties of cemented paste backfill under the influence of anionic polyacrylamide[J]. Chemosphere, 2022, 286: 131630.
[13] Fawell P D, Nguyen T V, Solnordal C B, et al. Enhancing gravity thickener feedwell design and operation for optimal flocculation through the application of computational fluid dynamics[J]. Mineral Processing and Extractive Metallurgy Review, 2021, 42(7): 496-510.
[14] Jeldres R I, Fawell P D, Florio B J. Population balance modelling to describe the particle aggregation process: A review[J]. Powder technology, 2018, 326: 190-207.
[15] Ruan Z, Li C, Shi C. Numerical simulation of flocculation and settling behavior of whole-tailings particles in deep-cone thickener[J]. Journal of Central South University, 2016, 23(3): 740-749.
[16] Grabsch A F, Fawell P D, Adkins S J, et al. The impact of achieving a higher aggregate density on polymer-bridging flocculation[J]. International Journal of Mineral Processing, 2013, 124: 83-94.
[17] Leiva W H, Fawell P D, Goñi C, et al. Temporal evolution of the structure of tailings aggregates flocculated in seawater[J]. Minerals Engineering, 2021, 160: 106708.
[18] Ruan Z, Wang Y, Wu A, et al. A theoretical model for the rake blockage mitigation in deep cone thickener: A case study of lead-zinc mine in China[J]. Mathematical Problems in Engineering, 2019, 2019.
[19] Hammerschmidt N, Engelmaier H, Dattenböck C, et al. Structured bottom section in inclined settlers for efficient continuous solid-liquid separation and washing of the solid fraction[J]. Separation and Purification Technology, 2021, 259: 118142.
[20] Schoenbrunn F, Bach M. The development of paste thickening and its application to the minerals industry; an industry review[J]. BHM Berg-und Hüttenmännische Monatshefte, 2015, 6(160): 257-263.
[21] Serbon J C, Mac-Namara L, Schoenbrunn F. Application of the FLSmidth deep cone technology to the fertilizer plants in OCP[J].

Procedia Engineering, 2016, 138: 314-318.
[22] Heath A, Barycki A, Baladron J. Vane feedwell flocculant sparger optimisation trial[C]//XXVII International Mineral Processing Congress (IMPC), Santiago, Chile. 2014.
[23] Johnson J, Accioly A. Feedwell is the heart of a thickener[C]//Paste 2017: Proceedings of the 20th International Seminar on Paste and Thickened Tailings. University of Science and Technology Beijing, 2017: 23-28.
[24] Heath A R, Triglavcanin R A. Advances in thickener feedwell design via computational fluid dynamics modelling[C]//XXV International Mineral Processing Congress (IMPC). 2010: 6-10.
[25] Fawell P D, Farrow J B, Heath A R, et al. 20 Years of AMIRA P266 “Improving Thickener Technology”—How has it changed the understanding of thickener performance?[C]//Paste 2009: Proceedings of the Twelfth International Seminar on Paste and Thickened Tailings. Australian Centre for Geomechanics, 2009: 59-68.
[26] Fawell P D, Simic K, Mohanarangam K, et al. Pilot and full-scale validation of thickener and feedwell modelling[C]//Paste 2011: Proceedings of the 14th International Seminar on Paste and Thickened Tailings. Australian Centre for Geomechanics, 2011: 81-91.
[27] Wu A, Ruan Z, Li C, et al. Numerical study of flocculation settling and thickening of whole-tailings in deep cone thickener using CFD approach[J]. Journal of Central South University, 2019, 26(3): 711-718.
[28] Ruan Z, Wu A, Bürger R, et al. A population balance model for shear-induced polymer-bridging flocculation of total tailings[J]. Minerals, 2021, 12(1): 40.
[29] Tanguay M, Fawell P, Adkins S. Modelling the impact of two different flocculants on the performance of a thickener feedwell[J]. Applied Mathematical Modelling, 2014, 38(17-18): 4262-4276.
[30] Wang X, Cui B, Zhao Q, et al. Particle flocculation in a stirred tank: A microscopic test by coupled CFD-DEM approach[J]. Journal of Environmental Chemical Engineering, 2022, 10(1): 107005.

[31] Wang X, Cui B, Wei D, et al. CFD-PBM modelling of tailings flocculation in a lab-scale gravity thickener[J]. Powder Technology, 2022, 396: 139-151.
[32] Wang X, Cui B, Wei D, et al. Effect of feed solid concentration on tailings slurry flocculation in a thickener by a coupled CFD-PBM modelling approach[J]. Journal of Environmental Chemical Engineering, 2021, 9(6): 106385.
[33] WANG X, CUI B, WEI D, et al. Effect of feed solid concentration on tailings slurry flocculation in a thickener by a coupled CFD-PBM modelling approach [J]. Journal of Environmental Chemical Engineering, 2021, 9(6): 106385.
[34] Jeldres M, Piceros E C, Toro N, et al. Copper tailing flocculation in seawater: Relating the yield stress with fractal aggregates at varied mixing conditions[J]. Metals, 2019, 9(12): 1295.
[35] Owen A T, Nguyen T V, Fawell P D. The effect of flocculant solution transport and addition conditions on feedwell performance in gravity thickeners[J]. International Journal of Mineral Processing, 2009, 93(2): 115-127.
[36] White R B, Sutalo I D, Nguyen T. Fluid flow in thickener feedwell models[J]. Minerals Engineering, 2003, 16(2): 145-150.
[37] Mohanarangam K, Nguyen T V, Stephens D W. Evaluation of two-equation turbulence models in a laboratory-scale thickener feedwell[C]//Seventh International Conference on Computational Fluid Dynamics in the Minerals and Process Industries. 2009: 9-11.
[38] Nguyen T V, Farrow J B, Smith J, et al. Design and development of a novel thickener feedwell using computational fluid dynamics[J]. Journal of the Southern African Institute of Mining and Metallurgy, 2012, 112(11): 939-948.
[39] Alireza A S, Ataallah S G, Majid E G, et al. Application of response surface methodology and central composite rotatable design for modeling the influence of some operating variables of the lab scale thickener performance[J]. International Journal of Mining Science and Technology, 2013, 23(5): 717-724.
[40] Luna F D T, Silva A G, Vianna Junior A S. The influence of geometry

on the fluid dynamics of continuous settler[J]. Open Journal of Fluid Dynamics, 2020, 10(3): 164-183.
[41] Costine A, Cox J, Travaglini S, et al. Variations in the molecular weight response of anionic polyacrylamides under different flocculation conditions[J]. Chemical Engineering Science, 2018, 176: 127-138.
[42] Owen A T, Fawell P D, Swift J D, et al. Using turbulent pipe flow to study the factors affecting polymer-bridging flocculation of mineral systems[J]. International Journal of Mineral Processing, 2008, 87(3-4): 90-99.
[43] Ortiz A, García J, Uggetti E, et al. Optimization of multi-stage thickening of biomass in a demonstrative full–scale microalgae-based wastewater treatment system[J]. Separation and Purification Technology, 2022, 281: 119830.
[44] Fawell P D, Costine A D, Grabsch A F. Why small-scale testing of reagents goes wrong[C]//Paste 2015: Proceedings of the 18th International Seminar on Paste and Thickened Tailings. Australian Centre for Geomechanics, 2015: 153-165.
[45] Farrow J B, Fawell P D, Johnston R R M, et al. Recent developments in techniques and methodologies for improving thickener performance[J]. Chemical engineering journal, 2000, 80(1-3): 149-155.
[46] Luna F D T, Silva A G, Fukumasu N K, et al. Fluid dynamics in continuous settler[J]. Chemical Engineering Journal, 2019, 362: 712-720.
[47] McMillan J, Shaffer F, Gopalan B, et al. Particle cluster dynamics during fluidization[J]. Chemical Engineering Science, 2013, 100: 39-51.
[48] Smith S J, Friedrichs C T. Image processing methods for in situ estimation of cohesive sediment floc size, settling velocity, and density[J]. Limnology and Oceanography: Methods, 2015, 13(5): 250-264.
[49] Maćczak P, Kaczmarek H, Ziegler-Borowska M. Recent achievements in polymer bio-based flocculants for water treatment[J].

Materials, 2020, 13(18): 3951.
[50] Fan Y, Ma X, Dong X, et al. Characterisation of floc size, effective density and sedimentation under various flocculation mechanisms[J]. Water Science and Technology, 2020, 82(7): 1261-1271.
[51] Šutalo I D, Paterson D A, Rudman M. Flow visualisation and computational prediction in thickener rake models[J]. Minerals Engineering, 2003, 16(2): 93-102.
[52] Alonso-Martínez M, Navarro-Manso A, Castro-Fresno D, et al. Improvement of a system for catchment, pretreatment, and treatment of runoff water using PIV tests and numerical simulation[J]. Journal of Irrigation and Drainage Engineering, 2014, 140(8): 04014028.
[53] Zhou T, Li M, Zhou C, et al. Numerical simulation and optimization of red mud separation thickener with self-dilute feed[J]. Journal of Central South University, 2014, 21(1): 344-350.
[54] Chang Q, Mao Y, Zeng L, et al. Flocculation Efficiency in Taylor-Couette Flow[J]. Journal of Materials Science and Chemical Engineering, 2016, 4(1): 1-7.
[55] Mao Y, Chang Q, Zeng L, et al. Velocity field structure and flocculation efficiency in Taylor-Couette flow[J]. Separation Science and Technology, 2013, 48(4): 659-663.
[56] Ruan Z, Wu A, Bürger R, et al. Effect of interparticle interactions on the yield stress of thickened flocculated copper mineral tailings slurry[J]. Powder Technology, 2021, 392: 278-285.
[57] Wang S N, Chen Y H, Ge R, et al. Revealing the hydrodynamic effects on phosphorus recovery as vivianite in stirring and aeration systems through PIV experiments and theoretical calculations[J]. Chemical Engineering Journal, 2023, 475: 146454.
[58] Nieto S, Toledo P G, Robles P, et al. Impact of magnesium on the flocculation, sedimentation and consolidation of clay-rich tailings in lime-treated seawater[J]. Separation and Purification Technology, 2023: 125633.
[59] Liang X, Wu M, Mu Y, et al. A multi-stage enhanced flocculation reactor for the treatment of simulated shale gas hydraulic fracturing flowback fluid: Effect of aspect ratios for the intense mixing

section[J]. Separation and Purification Technology, 2024, 330: 125488.
[60] Dong Y, Hua Z, Zhang Q, et al. Enhanced flocculation and sedimentation of copper tailings by polycarboxylate ether superplasticizer[J]. Separation and Purification Technology, 2023, 316: 123696.
[61] Najafabadi Z R, Soares J B P. Flocculation and dewatering of oil sands tailings with a novel functionalized polyolefin flocculant[J]. Separation and Purification Technology, 2021, 274: 119018.
[62] Quezada G R, Ramos J, Jeldres R I, et al. Analysis of the flocculation process of fine tailings particles in saltwater through a population balance model[J]. Separation and Purification Technology, 2020, 237: 116319.